Design of Machines and Structures, Vol. 13, No. 1 (2023), pp. 12–27.
https://doi.org/10.32972/dms.2023.002

STUDY THE EFFECT OF THE TOOTH CHAMFER ANGLE ON THE DOG CLUTCH SHIFTABILITY

AYHAM ALJAWABRAH[1], LÁSZLÓ LOVAS[2]

Budapest University of Technology and Economics,
Department of Railway Vehicles and Vehicle System Analysis
1111. Műegyetem rkp. 3, Budapest
[1]aaljawabrah@edu.bme.hu, [2]lovas.laszlo@kjk.bme.hu
[1]https://orcid.org/0000-0002-7537-6358, [2]https://orcid.org/0000-0001-6710-9084

Abstract: This paper studies the shiftability of the face dog clutch with chamfered teeth. The effect of the chamfer angle on the shiftability map and the probability are studied. In contrast to previous studies, a generalized mathematical model is developed based on the shiftability condition. The analysis considered two sets of cases: the overlap distance cases, and the chamfer side cases. The overlap distance cases locate the successful engagement position. The chamfer side cases investigate the effect of the system geometry and consider two cases. The results show that the chamfer angle has a negative effect on the dog clutch shiftability. Some geometric parameters show a different effect on the engagement probability for the rectangular tooth and chamfered tooth cases, and this behaviour is also analysed.

Keywords: *dog clutch, shiftability condition, shiftability map, engagement probability, chamfer angle*

1. INTRODUCTION

All vehicle systems receive great attention to improve its performance (Alzyod & Ficzere, 2021), (Alsardia, Lovas, & Ficzere, 2021), (Nguyen, Moghaddam, Pirouzfar, Fayyazbakhsh, & Su, 2021) and the vehicle gearbox is one of these systems. Conventional vehicle gearboxes utilize the synchronizer as a gearshift element to guarantee successful gearshift (Lovas, Play, Márialigeti, & Rigal, 2006). However, dog teeth clutch has been replacing the synchromesh because it has quicker shifting time, simpler structure, larger power transmitting capacity, and lower cost (Shiotsu, et al., 2019). The dog clutch is being applied in automated manual transmissions (Bóka, Márialigeti, Lovas, & Trencséni, 2009), automatic

transmissions (Duan, 2014), and clutchless automated manual transmissions (Walker, Fang, & Zhang, 2017).

As dog teeth clutch is only a clutch and not a synchronizer, the problems of synchronization and shiftability have to be resolved. Boka et al. (Bóka, Márialigeti, Lovas, & Trencséni, 2010) used the notion of engagement probability to find a certain successful region depending on the initial mismatch speed of the clutch halves. However, they focused on the low mismatch speed zone in their research and did not investigate the large mismatch speeds.

In a previous paper (Aljawabrah & Lovas, 2023), we have studied the dog teeth clutch shiftability from a kinematic point of view and determined the shiftability condition that identifies the successful engagement regions. We showed the parameters affecting the shiftability and determined the shiftability map based on an analytical method. In another previous paper (Aljawabrah & Lovas, 2022) we developed a method to calculate the shifting probability and studied the engagement probability's sensitivity to the system parameters. We showed that the number of teeth, and the amount of the tangential backlash affect positively the engagement probability, while the initial mismatch speed and the overlap distance, being the required tooth overlap for successful engagement, have a negative effect. All the aforementioned studies considered the dog tooth to be rectangular, not chamfered. The effect of the chamfer angle for the tooth edge on the dog teeth clutch shiftability is rarely discussed in the literature.

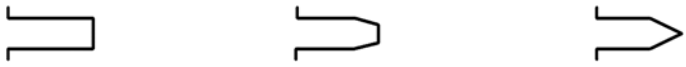

a) b) c)

Figure 1 *Tooth geometry for a) rectangular (no chamfer) tooth, b) partially chamfered tooth, and c) fully chamfered tooth*

Among these rare cases, (Duan, 2014) developed a mathematical dynamic model for the dog teeth clutch used in an automatic transmission, and the model considered chamfered tooth. Eriksson (Mehari, Eriksson, & Kuttikal, 2013) performed a multibody dynamic parametric study for the dog clutch used in a truck gearbox transfer case. He studied three different tooth designs to study the effect of the chamfer distance, chamfer angles, and tooth side edge's angle. and the number of teeth. He developed eight sets of parameter combinations for simulation. Andersson (Andersson & Goetz, 2010) performed dynamic FEA using Abaqus on the dog clutch to investigate the effect of the chamfer angle, chamfer distance, and tooth angle. The aim was to find the maximum relative rotational speed that the system can handle to have a successful gearshift for each geometry and to

determine the best geometry among eleven alternatives. The author claimed that engagement is easier if the chamfer angle is smaller. Moreover, a fully chamfered tooth, Figure 1 c, is more effective than a partially chamfered tooth, Figure 1 b, for the same chamfer angle. These studies have considered the effect of the tooth chamfer angle using either dynamic modelling, multibody or FEA. These approaches require complicated models and are slow to compute. Moreover, the number of studied cases is limited.

This work aims to develop a method to investigate the effect of the tooth chamfer angle on the dog clutch shiftability. A generalized shiftability condition is developed based on (Aljawabrah & Lovas, 2023), where the chamfered tooth geometry is added to the previously developed model. A mathematical model taking into account the effect of the chamfer to the shiftability condition is presented. The shiftability map is created for different chamfer angle values, based on the method described in (Aljawabrah & Lovas, 2022), and different cases for the overlap distance and the chamfer angle parameters are examined. Finally, the effect of geometric parameters on the engagement probability for chamfered and rectangular tooth cases is compared.

2. METHODOLOGY

In a previous paper (Aljawabrah & Lovas, 2023), we have presented the dog clutch geometry, and the main geometric and kinematic parameters. Further on, we introduced a kinematical shiftability condition that guarantees side impact-free gearshift. Here, the considered tooth geometry had no chamfers.

The dog teeth clutch geometry is presented in detailed in Figure 2. The dog clutch (Figure 2 a) is a coupling used to transmit power. It consists of two parts having complementary geometry. These complementary shapes are referred to as dog teeth.

The parameters of the clutch geometry are presented in Table 1. The tooth dog geometry is discussed along two directions. Figure 2 b shows a linear (tangential) representation and Figure 2 c shows a radial representation. At the beginning of the shifting, an axial gap x_0 exists between the sliding sleeve and the shifted gear, and there is an initial relative angular position ξ between the marked teeth. Here the sliding dog can slide axially with a speed v_0, while it has relative angular rotation with respect to the target gear. The relative angular rotation is called the mismatch speed $\Delta\omega_0$. The engagement of the complementary geometries is eased with an angular backlash.

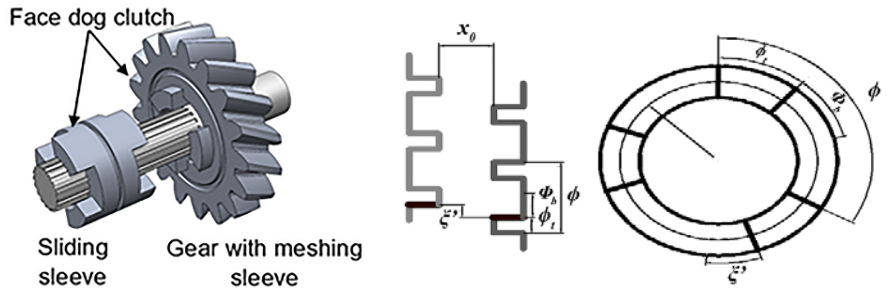

a) b) c)

Figure 2 *Face dog clutch: a) 3D model, and geometry as b) linear, and c) radial representation (Aljawabrah & Lovas, Kinematical Model of the Dog Clutch Shifting, 2023)*

The axial dog clutch has an angular pitch ϕ given by (1), and an angular backlash given according to (2), where ϕ_t is the tooth thickness angle.

$$\phi = \frac{2\pi}{z} \tag{1}$$

$$\Phi_b = \phi - 2\phi_t \tag{2}$$

Table 1
Dog clutch shiftability parameters

Parameter	**Range**	**Fixed Value**	**Parameter**	**Range**	**Fixed Value**
Initial relative position ξ_0 [°]	0-ϕ	0	Axial gap x_0 [mm]	1-6	7
Mismatch speed $\Delta\omega_0$ [rad] ([min-1])	0-500 (0 4775)	20 (190)	Overlap distance x_{fed} [mm]	0.5-3	0.5
Axial Speed v_0 [mm/s]	0-500	250	Number of teeth Z [-]	2-10	10
Mean radius r [mm]	5-60	40	Angular backlash Φ_b [°]	2-30	25

In (Aljawabrah & Lovas, 2023) we have studied the dog clutch shiftability for rectangular tooth dog clutch. We suppose that a successful engagement happens when an overlap x_{fed} is reached in the axial direction, where the a tooth on the sliding sleeve overlap a tooth on the gear with a distance x_{fed}, and based on this, we developed the shiftability condition shown in (3). This condition combines all

kinematic and geometric parameters and determines if there is a possibility of successful shifting for a given set of parameters. This condition was the base to develop the shiftability map and calculate the shifting probability as described in (Aljawabrah & Lovas, 2022).

$$0 \leq mod\ \left(\xi_0 + \Delta\omega_0 \frac{x_0}{v_0}, \frac{2\pi}{z}\right) \leq \Phi_b - \Delta\omega_0 \frac{x_{fed}}{v_0} \tag{3}$$

The shiftability condition was developed for teeth with no chamfer. The application for chamfered teeth requires the modification of some parameters. Figure 3a shows the geometry for the tooth chamfer with a chamfer angle (β). The chamfer length (x_{ch}) can be connected to the tooth thickness by (4). Solving (2) for ϕ_t and substituting into (4), (5) can be obtained.

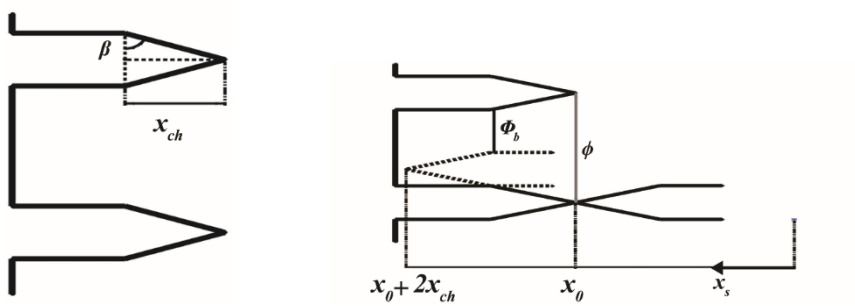

a) b)

Figure 3 *a) Geometry of chamfered dog tooth, b) Backlash variation*

$$x_{ch} = \frac{\phi_t r}{2} \tan(\beta) \tag{4}$$

$$x_{ch} = \frac{\left(\frac{2\pi}{z} - \Phi_b\right) r}{4} \tan(\beta) \tag{5}$$

In the case of a not chamfered tooth, the angular backlash (Φ_b) is constant as the sliding dog moves axially. The introduction of the chamfer causes the backlash to decrease while the sliding dog moves axially towards the gear wheel (Figure 3 b). A generalized equation can be formulated for the backlash in function of the axial position. According to Figure 3 b, the backlash equals ϕ at $x = x_0$ and equals Φ_b at $x = x_0 + 2x_{ch}$. So, a linear relationship can be derived as shown in (6). Substituting (1) and (5) into (6), (7) can be formed.

$$\Phi_b(x) = \phi - \frac{x - x_0}{2x_{ch}}(\phi - \Phi_b) \quad x_0 \le x \le x_0 + 2x_{ch} \tag{6}$$

$$\Phi_b(x) = \frac{2\pi}{z} - 2\frac{x - x_0}{r \tan(\beta)} \tag{7}$$

In what follows, we consider chamfer angle values only within the interval [0°;45°]. The analysis of the effect of the chamfer angles considers two distinct sets of cases: the chamfer sides cases, and the successful connection position (required overlap distance).

Firstly, let us consider the chamfer sides cases set. Here, two cases are considered: firstly, just one tooth with side chamfer and the another without, and both teeth having chamfer (Figure 4). The successful engagement position is considered at full overlap distance for both cases, as illustrated in (8). The backlash at full overlap distance is Φ_b.

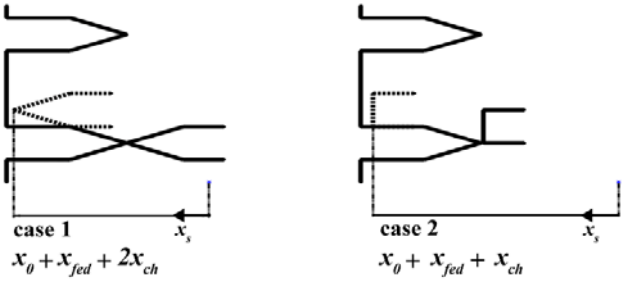

Figure 4 *Chamfer side cases*

$$x_{fed}{}' = \begin{cases} x_{fed} + 2x_{ch} & case\ 1 \\ x_{fed} + x_{ch} & case\ 2 \end{cases} \tag{8}$$

Secondly, let us consider the successful connection position cases. Figure 5 shows the successive steps to reach the successful connection position. In the case of not chamfered (rectangle) tooth case, the overlap distance has a clear definition, as it depends on the wear of the tooth vertices, and it can be identified experimentally. A successful gearshift process is guaranteed if the sliding sleeve can pass the overlap distance without teeth face impact, and this distance is what we refer to as the 'successful connection position'. Knowing the successful connection position and other system parameters, successful gearshift process can be distinguished based on (3). However, in case of chamfered tooth geometry, the face impact can happen at different places, and it is unknown at which location the face impact will no

longer affect the gearshift process. In other words, it is not clearly defined at which connection position the sliding sleeve will not bounce back and engage with the gear sleeve even though a face impact occurs after this position. To understand the system, three successful connection position cases are considered, where these cases aim to identify possible successful connection positions. These positions are directly connected to the chamfer angle, so they can assist to study the effect of the chamfer angle both on the shiftability map and the engagement probability.

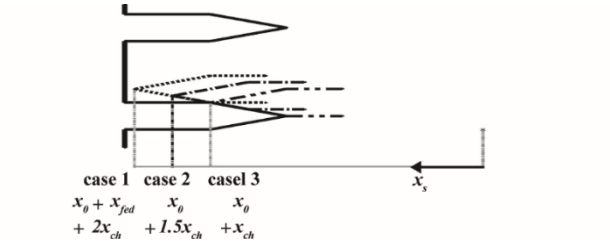

Figure 5 *Successful connection position cases*

The three cases for the overlap distance, shown in (9), are the following: full overlap distance (case 1), the overlap distance is 1.5 times the chamfer length (case 2), and the overlap distance equals the chamfer length (case 3). As the backlash changes with the axial position, the backlash values at the successful engagement position are used as illustrated in (10). This equation shows that an expression for the backlash can be derived without depending on the chamfer angle. This is expected, since from the backlash equation derivation (6) we see that the equation is based on the chamfer length (x_{ch}), and the overlap distance ($x_{fed}{}'$) is also described in terms of chamfer length (x_{ch}). Substituting all in (6), the x_{ch} terms can be eliminated.

$$x_{fed}{}' = \begin{cases} x_{fed} + 2x_{ch} & case\ 1 \\ 1.5x_{ch} & case\ 2 \\ x_{ch} & case\ 3 \end{cases} \tag{9}$$

$$\Phi_b{}' = \begin{cases} \Phi_b & case\ 1 \\ \frac{2\pi}{z} - \frac{1.5}{2}\left(\frac{2\pi}{z} - \Phi_b\right) & case\ 2 \\ \frac{2\pi}{z} - \frac{1}{2}\left(\frac{2\pi}{z} - \Phi_b\right) & case\ 3 \end{cases} \tag{10}$$

From (8), (9), (10) it is clear that the modified parameters are the overlap distance for the two case sets, as well as the backlash for the second case set, but the backlash does not depend on the chamfer angle. So, in the following discussion, the focus will be on the overlap distance ($x_{fed}{}'$).

3. RESULTS

The chamfer angle has a great effect on the overlap distance. Figure 6 shows x_{fed}' response to the chamfer angle. For chamfer sides' cases, Figure 6 a shows higher overlap distance for two sides chamfer case compared to one side chamfer. According to (5), x_{ch} increases with higher β, which in term increases the required tooth overlap distance, as (8) shows. Also, considering Figure 6 b, case 1 (full x_{fed}) has higher sensitivity to β, compared with case 2 (x_{fed}' is 1.5xch) and case 3 (x_{fed}' is x_{ch}) which agrees with (9). Below 15° chamfer angle, case 2 and case 3 have lower x_{fed}' compared to no chamfer case.
It has been shown that the chamfer angle affects the overlap distance, which in term will affect the shiftability map and the engagement probability. So, it is worth to briefly explaining how this distance affects the dog clutch shiftability.
Figure 8 shows the so-called shiftability map where the blue zone expresses the successful gearshift region where (3) is evaluated at each point in a given domain, knowing all the parameters appearing in this equation. In (Aljawabrah & Lovas, 2022) we showed that higher overlap distance narrows the successful engagement area, and this behaviour is clear in Figure 7 a, where the successful region portion from a given domain decays rapidly with x_{fed}.

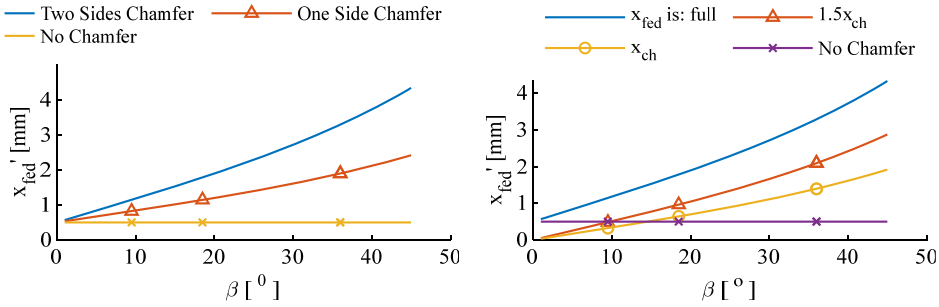

a) b)

Figure 6 *Chamfer angle effect on the overlap distance for a) chamfer sides cases, and b) for overlap distance cases*

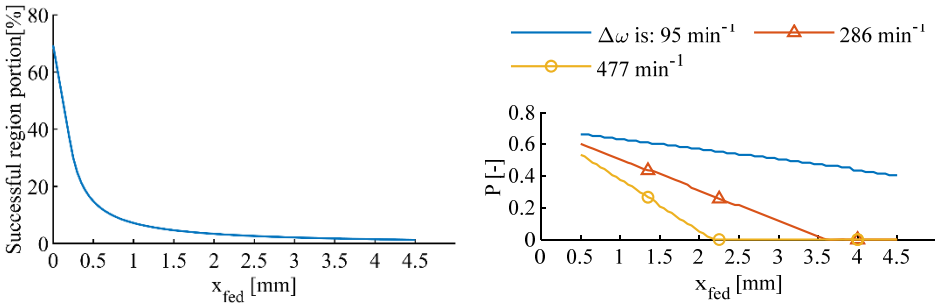

a) b)

Figure 7 *Overlap distance effect on a) successful engagement area, and b) engagement probability*

On the other hand, in many cases, the initial relative position cannot be measured. So, the initial relative position is considered to be a random variable in the interval [0, ϕ], or one tooth pitch period, and in contrast to the shiftability condition in (3), the successful gearshift process is described by engagement probability. Figure 7 b shows the probability sensitivity to x_{fed} change. Here the probability decreases with a higher overlap distance, and theoretically, there is no possible connection above a certain value, as the required time to cover x_{fed} becomes larger than the available time before the gear's and sliding sleeve's teeth impact.

3. 1. Chamfer sides' cases

Let us consider the cases when chamfers exist or not on the mating teeth (Figure 4). In Figure 8, the horizontal axis shows ξ and $\Delta\omega_0$ is on the vertical axis. The maps represent chamfer existence cases 1, and 2 for different chamfer angle β. The third column of the subfigures in Figure 8 shows the no chamfer case for reference. Here, with the increase of β, the zone of successful shifting (blue zones) decreases. Referring to Figure 6 a, x_{fed}' increases with higher chamfer angle values, which increases the required overlap distance x_{fed}'.

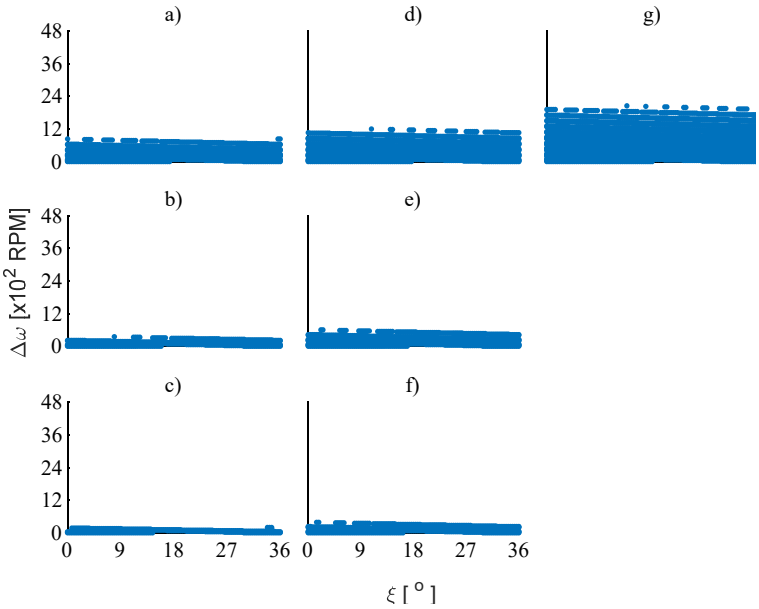

Figure 8 *The shiftability map for ξ_0 and $\Delta\omega$ at different chamfer side cases: one side chamfer case for β of a) 10° b) 30° c) 45° and two sides chamfer case for β of d) 10° e) 30° f) 45°, and e) no chamfer case*

When comparing case 1 to case 2, it can be seen that the latter has larger successful engagement regions at a fixed chamfer angle, since case 2 has a shorter overlap distance (Figure 8). Moreover, the difference in the shiftability map between case 1 and case 2 decreases at higher β. Figure 6 a shows that x_{fed}' increases rapidly with increasing β. Note also, that with increasing x_{fed}', the system approaches the no shiftability point, as the size of the blue zone decreases on the shiftability map, Figure 7 a.

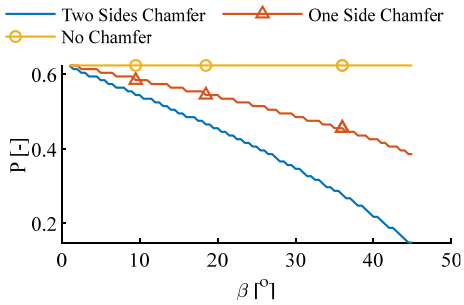

Figure 9 *Engagement probability for chamfer side cases, ξ_0 is random in the interval [0, ϕ]*

Figure 9 shows that the engagement probability decreases for both two and one chamfer cases as the overlap distance increases. Note also, that the probability has higher sensitivity at higher β. Figure 6 a shows the x_{fed}' is more sensitive β at higher values which gives higher probability sensitivity at higher chamfer angles.

3. 2. Successful connection position cases

Figure 10 shows shiftability maps. The horizontal axis shows ξ_0 and $\Delta\omega_0$ is on the vertical axis. The maps represent x_{fed}' cases 1, 2, and 3 for different chamfer angles β. Case 3 has the largest successful engagement region at fixed β; case 3 has the shortest overlap distance compared with case 2 and case 1 as Figure 10 shows. It can also be seen that the successful engagement regions (blue zones) decrease with higher chamfer angles.

The shiftability maps are more sensitive to the change in the chamfer angle (β) in case 3 and have less effect on case 2 shiftability maps, but the lowest effect on case 1. Figure 6 b shows that case 3 has shorter x_{fed}' compared to the other two cases and as Figure 7 a shows that the successful region portion is more sensitive to the change in x_{fed} at lower values. The phenomenon is similar to that seen in Figure 8, since mainly the chamfer angle affects the overlap distance in both cases set.

Figure 11 illustrates the engagement probability for the overlap distance cases, when the mismatch speed increases. The probability decreases with the β as expected. Case 1 has the lowest probability since it has the highest x_{fed}'. Case 3 probability curves' decrease is the quickest, then comes case 2, then the case 1. This means that having a chamfer limits the possibility of successful shifting at higher mismatch speed domain. This is justified with Figure 11: x_{fed}' increases with β increase, which causes the shifting probability to decrease. Moreover, the

probability curve trends are similar to those in Figure 9 since the chamfer angle mainly affects the overlap distance.

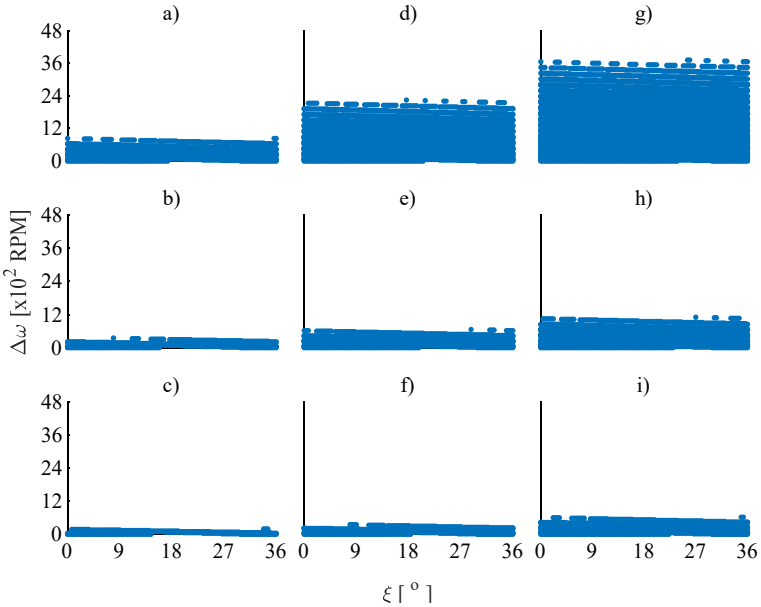

Figure 10 *The shiftability map for ξ_0 and $\Delta\omega$ at different overlap distance cases: Full x_{fed}' (case 1) for β of a) 10° b) 30° c) 45°, x_{fed}' is 1.5x_{ch} (case 2) for β of d) 20° e) 30° f) 45°, x_{fed}' is x_{ch} (case 3) for β of g) 20° h)30° i) 45°*

Figure 11 a also shows that case 3 always has a higher probability compared to no chamfer case at given low mismatch speed. However, this advantage vanishes with the mismatch speed increase. Thus, the developed model allows to check whether it is worth to have a chamfer at given tooth geometry and mismatch speed conditions.

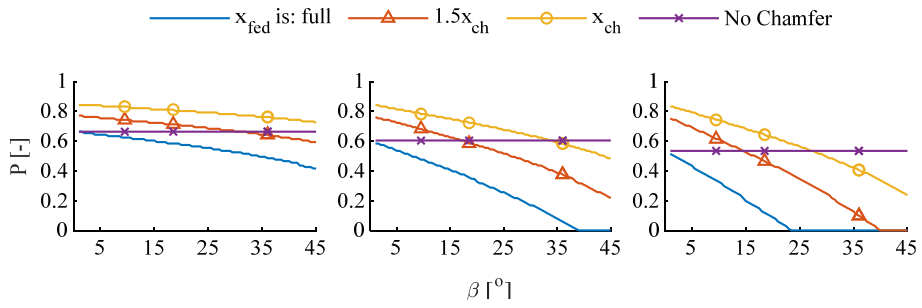

a) b) c)

Figure 11 *Probability plot for overlap distance cases when $\Delta\omega_0$ is a) 95 min^{-1} b) 286 min^{-1} and c) 477 min^{-1}, ξ_0 is random in the interval [0, ϕ]*

3. 3. System Parameters effect

(5) describing the chamfer length contains geometric parameters: the mean tooth radius r, the number of teeth z, and the angular backlash Φ_b. In what follows, the effect of these parameters on the engagement probability in the case of a rectangular and chamfered tooth are compared.

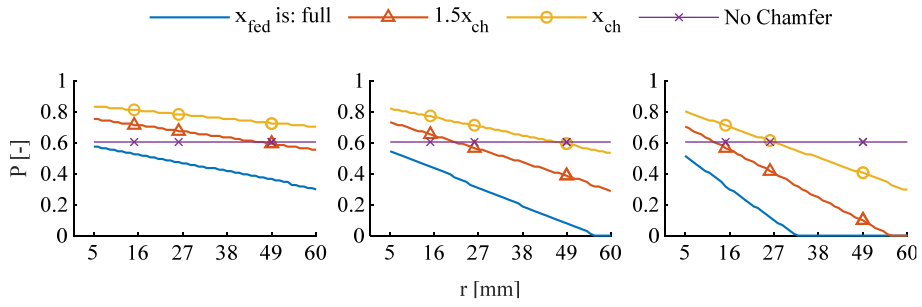

a) b) c)

Figure 12 *Probability sensitivity to the men radius change for β of a) 15° b) 30° and c) 45°, ξ_0 is free in the interval [0, ϕ]*

a) b) c)

Figure 12 shows that the radius has no effect on the connection probability in case there is no chamfer, but has a negative linear effect if the dog teeth are chamfered even at fixed β. According to (5), the chamfer length increases with the mean radius, as well as the tooth thickness. Comparison of Figure 12 a, b, and c, show

that the slope of the curves is increasing, which means probability sensitivity for the mean radius increases as the β increases.
Figure 13 a illustrates the effect of the number of teeth z on the connection probability. The trends of the curves in Figure 13 a, b, and c show that teeth number has a direct linear relationship with probability.
On the other hand, increasing β increases the minimum required number of teeth to have a possible gearshift.

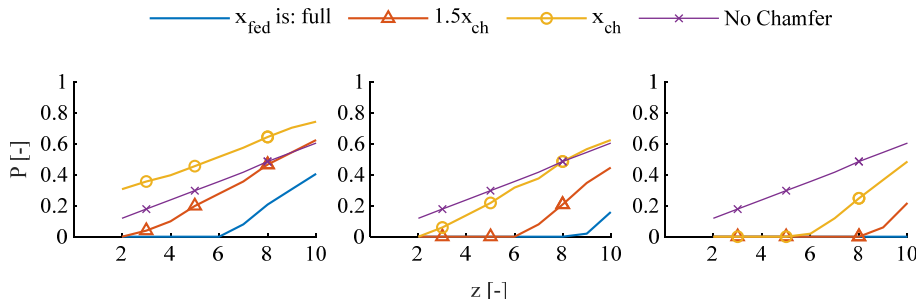

a) b) c)

Figure 13 *Probability sensitivity to the number of teeth change for β of a) 15° b) 30° and c) 45°*

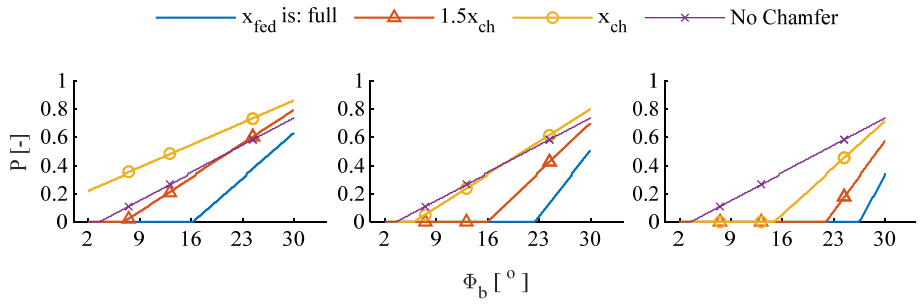

a) b) c)

Figure 14 *Probability sensitivity to backlash change for β of a) 15° b) 30° and c) 45°*

Figure 14a) b) c)

Figure 14 illustrates the change in the connection probability depending on the angular backlash. The probability curve trends are similar to those in Figure 13, and similar conclusions can be drawn. On the other hand, the tooth thickness has

a major effect on the chamfer length as shown in (4): the chamfer length increases with the tooth thickness. So, reducing the tooth thickness within the angular pitch has a positive effect on the engagement probability by reducing the chamfer length from one side, and allowing for higher backlash from another side.

4. Summary

In this paper, the effect of the chamfer angle on the shiftability map and the engagement probability was investigated. The analysis is based on the kinematical shiftability condition. The inclusion of the chamfer angle modified the expression of the overlap distance and the backlash in the condition. The analysis considered two sets of cases: the overlap distance cases, and the chamfer side cases. The overlap distance cases try to locate the successful engagement position since the location is not clear compared to the rectangular tooth case while the chamfer side distance investigates the effect of the system geometry. Regarding the considered cases, the results showed a globally negative effect for the chamfer angle presence on the engagement probability, at fixed other parameters.
In case of low mismatch speeds, there may be some advantage in the application of chamfered teeth, but this zone is limited. At higher mismatch speeds, higher actuator axial speed must be present to overcome the overlap distance increase due to the chamfers.

References

Aljawabrah, A., & Lovas, L. (2022). Shiftability Study of a Dog Clutch., *VII. Gépészeti Szakmakultúra Konferencia.* Budapest. Retrieved from https://gteportal.eu/content/uploads/2022/09/1A_2_Lovas-Aljawabrah_Study_CIKK.pdf

Aljawabrah, A., & Lovas, L. (2023). Kinematical Model of the Dog Clutch Shifting. *GÉP, 74*(1), 9-12.

Alsardia, T., Lovas, L., & Ficzere, P. (2021). Prototype for fit investigations. *Design of Machines and Structures, 11*(1), 5-15. doi:https://doi.org/10.32972/dms.2021.001

Alzyod, H., & Ficzere, P. (2021). Potential applications of additive manufacturing technologies in the vehicle industry. *Design of Machines and Structures, 11*(2), 5-13. doi:http://doi.org/10.32972/dms.2021.009

Andersson, M., & Goetz, K. (2010). FE analysis of a dog clutch for trucks with all-wheel-drive. *Master thesis*. Växjö, Sweden: Linnaeus University.

Bóka, G., Márialigeti, J., Lovas, L., & Trencséni, B. (2009). External synchronization strategies for automated mechanical transmissions with face dog clutch and countershaft brake. *Scientific Bulletin Series C: Fascicle Mechanics, Tribology, Machine Manufacturing Technology, 224*(9), 75-80. doi:https://doi.org/10.1243/09544070JAUTO1435

Bóka, G., Márialigeti, J., Lovas, L., & Trencséni, B. (2010). Face dog clutch engagement at low mismatch speed. *Periodica Polytechnica Transportation Engineering, 38*(1), 29-35. doi:https://doi.org/10.3311/pp.tr.2010-1.06

Duan, C. (2014). Analytical study of a dog clutch in automatic transmission application. *SAE International Journal of Passenger Cars-Mechanical Systems, 7*(3), 1155-1162. doi:https://doi.org/10.4271/2014-01-1775

Lovas, L., Play, D., Márialigeti, J., & Rigal, J.-F. (2006). Modeling of gear changing behaviour. *Periodica Polytechnica Transportation Engineering, 34*(1-2), 35-58.

Mehari, A., Eriksson, F., & Kuttikal, J. L. (2013). Parametric study of a dog clutch used in a transfer case for trucks. *Master thesis*. Växjö, Sweden: Linnaeus University.

Nguyen, D. D., Moghaddam, H., Pirouzfar, V., Fayyazbakhsh, A., & Su, C.-H. (2021). Improving the gasoline properties by blending butanol-Al2O3 to optimize the engine performance and reduce air pollution. *Energy, 218*. doi:https://doi.org/10.1016/j.energy.2020.119442

Shiotsu, I., Tani, H., Kimura, M., Nozawa, Y., Honda, A., Tabuchi, M., . . . Kanzaki, K. (2019). Development of High Efficiency Dog Clutch with One-Way Mechanism for Stepped Automatic Transmissions. *International Journal of Automotive Engineering, 10*(2), 156-161.

Walker, P. D., Fang, Y., & Zhang, N. (2017). Dynamics and control of clutchless automated manual transmissions for electric vehicles. *Journal of Vibration and Acoustics, 139*(6), 061005 (13 pages). doi:https://doi.org/10.1115/1.4036928